

# Successive Cancellation Automorphism List Decoding of Polar Codes

Lucas Johannsen<sup>\*†</sup>, Claus Kestel<sup>\*</sup>, Marvin Geiselhart<sup>‡</sup>, Timo Vogt<sup>†</sup>, Stephan ten Brink<sup>‡</sup> and Norbert Wehn<sup>\*</sup>

<sup>\*</sup> RPTU Kaiserslautern-Landau, 67663 Kaiserslautern, Germany,

<sup>†</sup> Koblenz University of Applied Sciences, 56075 Koblenz, Germany,

<sup>‡</sup> Institute of Telecommunications, University of Stuttgart, 70569 Stuttgart, Germany

Email: {lucas.johannsen, kestel, norbert.wehn}@rptu.de, {johannsen, vogt}@hs-koblenz.de,

{geiselhart,tenbrink}@inue.uni-stuttgart.de

**Abstract**—The discovery of suitable automorphisms of polar codes gained a lot of attention by applying them in Automorphism Ensemble Decoding (AED) to improve the error-correction performance, especially for short block lengths. This paper introduces Successive Cancellation Automorphism List (SCAL) decoding of polar codes as a novel application of automorphisms in advanced Successive Cancellation List (SCL) decoding. Initialized with  $L$  permutations sampled from the automorphism group, a superposition of different noise realizations and path splitting takes place inside the decoder. In this way, the SCAL decoder automatically adapts to the channel conditions and outperforms the error-correction performance of conventional SCL decoding and AED. For a polar code of length 128, SCAL performs near Maximum Likelihood (ML) decoding with  $L=8$ , in contrast to  $M=16$  needed decoder cores in AED. Application-Specific Integrated Circuit (ASIC) implementations in a 12 nm technology show that high-throughput, pipelined SCAL decoders outperform AED in terms of energy efficiency and power density, and SCL decoders additionally in area efficiency.

**Index Terms**—Polar Code, Automorphisms, Successive Cancellation List Decoding, 12 nm FinFET, ASIC Implementation

## I. INTRODUCTION

In the enhanced mobile broadband (eMBB) scenarios of the 5G New Radio (NR) standard, polar codes [1] were selected as error-correction codes for the control channels [2]. Polar codes achieve the capacity of binary memoryless channels under low-complexity Successive Cancellation (SC) decoding at infinite code length. However, SC decoding suffers from a poor error-correction performance in the practical block length regime. More advanced decoding algorithms, with Successive Cancellation List (SCL) decoding [3] being the most prominent one, were developed to overcome this limitation at the price of higher decoding complexity and implementation costs. However, SCL decoding approaches Maximum Likelihood (ML) decoding performance with sufficient large list size  $L$ .

Recently, Automorphism Ensemble Decoding (AED) [4] for polar codes [5]–[7] gained attention as a new ML-approaching algorithm. In AED, an ensemble of  $M$  low-complexity decoders (e.g., SC) operates on different permutations from the code’s automorphism group in parallel. The most probable code word is selected as output from the  $M$  constituent

decoders, which improves the overall error-correction performance.

In [8], near-ML performance was achieved for Reed-Muller (RM) codes by running SCL decoders on permutations of the channel Log-Likelihood Ratios (LLRs) corresponding to stage-shuffled factor graphs and combining the different lists in each decoding step. This approach was generalized in [9] by initializing the  $L$  decoding paths by permutations randomly sampled from the full automorphism group of the RM code.

The automorphism group of polar codes and its properties were investigated in [4]–[7]. Through the discovery of suitable automorphisms for polar codes, also more advanced polar decoding algorithms, e.g., SCL decoding, can be leveraged. The new contributions of this work are summarized as follows:

- We propose Successive Cancellation Automorphism List (SCAL) decoding of polar codes as a novel method to beneficially utilize permutations selected from the code’s automorphism group in the SCL decoding algorithm.
- We analyze the evolution of these permutations during SCAL decoding and provide simulation results to show the capability of channel adaption and the improved error-correction performance, respectively.
- We present implementation results of the proposed SCAL decoder architecture in a 12 nm FinFET technology and compare them with state-of-the-art, high-throughput AED and SCL decoders.

The remainder of this paper is structured in four sections: Section II describes the fundamentals of polar codes and the relevant decoding strategies. The new SCAL decoding algorithm is presented in Section III. Results with respect to an analysis of the evolution of the input permutations, the error-correction performance of SCAL decoding and its hardware implementation costs are provided in Section IV. Section V concludes this work.

## II. BACKGROUND

### A. Polar Codes

A polar code  $\mathcal{P}(N, K)$  [1] is a linear block code with code length  $N = 2^n$  and  $K$  information bits. The information set  $\mathcal{I}$  defines the row indices to obtain the generator matrix  $\mathbf{G}$  as the rows of  $\mathbf{G}_N = \mathbf{G}_2^{\otimes n}$ , where  $\mathbf{G}_2 = \begin{bmatrix} 1 & 0 \\ 1 & 1 \end{bmatrix}$  denotes

The authors acknowledge the financial support by the Federal Ministry of Education and Research of Germany in the project “Open6GHub” (grant numbers: 16KISK019 and 16KISK004).

the polarization kernel and  $\otimes n$  denotes the  $n$ -th Kronecker power. The codeword can be obtained from an input vector  $\mathbf{u}$  as  $\mathbf{x} = \mathbf{u}\mathbf{G}_N$ , where  $\mathbf{u}$  contains  $K$  information bits at the positions of  $\mathcal{I}$  and  $N - K$  frozen bits (set to 0) at the positions of  $\mathcal{F} = \mathcal{I}^C$ . Polar codes can also be seen as monomial codes. In particular, most practical polar codes are decreasing monomial codes, i.e., all sub-channels in  $\mathcal{I}$  obey the partial order according to [10], and are thus called decreasing polar codes. They are completely defined by the minimal information set  $\mathcal{I}_{\min}$  [5].

### B. Successive Cancellation Based Decoding

Polar code decoding can be represented as traversal of a balanced binary tree, the Polar Factor Tree (PFT) [11]. Input to the root node are the channel LLRs, defined as  $\text{LLR}(y_i) = \log(P(y_i|x_i = 0)/P(y_i|x_i = 1))$ , calculated from the  $N$  received channel values  $\mathbf{y}$  with  $i \in [0, N)$ . A node  $v$  in layer  $s$  receives a vector  $\boldsymbol{\alpha}^v$  of  $N_v = 2^s$  LLRs from its parent node in layer  $s + 1$ . The min-sum formulations of  $f$ - and  $g$ -functions [12] are used to obtain the messages passed to the left and the right child nodes,  $\boldsymbol{\alpha}^l$  and  $\boldsymbol{\alpha}^r$ , respectively. The partial-sum vector  $\boldsymbol{\beta}^v$  is returned to the parent node and calculated by the  $h$ -function combining  $\boldsymbol{\beta}^l$  and  $\boldsymbol{\beta}^r$ . Thus, SC-based decoding causes a depth first traversal of the PFT with an inherent priority to the left child. In the  $N$  leaf nodes,  $\boldsymbol{\beta}^v$  is set to the value of the estimated bit  $\hat{u}_i$  as

$$\hat{u}_i = \begin{cases} 0, & \text{if } i \in \mathcal{F} \text{ or } \alpha_i^v \geq 0 \\ 1, & \text{otherwise.} \end{cases} \quad (1)$$

### C. Successive Cancellation List Decoding

In SCL decoding [3], lists of  $L$  vectors are passed among the nodes of the PFT instead of only passing vectors  $\boldsymbol{\alpha}$  and  $\boldsymbol{\beta}$ . Therefore,  $l \in [0, L)$  is introduced to index the  $L$  concurrent paths, e.g., the LLRs of a node  $v$  are denoted as  $\alpha^{v,l}$ . For an information bit estimation in layer  $s = 0$  of the PFT, the decoding path splits, i.e., both possible values, 0 and 1, are considered. Consequently, an information bit estimation doubles the number of decoding paths. Unreliable paths must be rejected by sorting, when the number of paths exceeds  $L$ . For this purpose, every bit estimation updates a Path Metric (PM) to rate the reliability of each path. These PMs are initialized with 0 in LLR-based SCL decoding [13]. The PM of a path with index  $p \in [0, 2L)$  proceeding input path  $l \in [0, L)$  is updated for the  $i$ -th bit estimation by

$$\text{PM}_i^p = \begin{cases} \text{PM}_{i-1}^l + |\alpha_i^{v,l}|, & \text{if } \beta_i^{v,l} \neq \text{HDD}(\alpha_i^{v,l}) \\ \text{PM}_{i-1}^l, & \text{otherwise,} \end{cases} \quad (2)$$

with Hard Decision Decoding (HDD) on  $\alpha^v$  defined as

$$\text{HDD}(\alpha_i^{v,l}) = \begin{cases} 0 & \text{if } \alpha_i^{v,l} \geq 0 \\ 1 & \text{otherwise.} \end{cases} \quad (3)$$

Consequently, the PM is a cost function and, thus, the smallest PMs values belong to the most probable paths which survive the sorting step. The most probable path is selected as the output of the decoder after the last bit decision.

### D. Automorphisms for Polar Code Decoding

Automorphisms are permutations that map every code word onto another code word. It was shown that the group of affine automorphisms of decreasing polar codes equals the Block Lower-Triangular Affine (BLTA) group [6] defined as

$$\mathbf{z}' = \mathbf{A}\mathbf{z} + \mathbf{b}, \quad (4)$$

where  $\mathbf{A}$  is an invertible, block lower triangular binary matrix,  $\mathbf{b}$  an arbitrary binary vector and  $\mathbf{z}, \mathbf{z}'$  are the binary representations of the bit indices before and after permutations, respectively [4]. In [5], an algorithm to determine the block profile of  $\mathbf{A}$  for a given  $\mathcal{I}$  is provided. To select proper permutations  $\pi_m$  from the automorphism group, a greedy selection method was proposed in [14] to pick  $M$  permutations from different partitions of the automorphisms, i.e., the Equivalence Class (ECs) [7].

## III. SUCCESSIVE CANCELLATION AUTOMORPHISM LIST DECODING

Permuting the received channel data according to automorphisms corresponds to different noise realizations. Since there may be permutations that are easier to decode, the probability of finding the correct code word is increased in AED [4]. Simultaneously, AED benefits from the locality of the  $M$  independent, constituent ensemble decoder cores resulting in decreased hardware implementation costs compared to SCL decoders [14].

SCL decoding, on the contrary, splits the decoding paths  $\zeta$  whenever an information bit is decoded to overcome error propagation [3]. In a *Sort & Select* step, a message exchange takes place to proceed the  $L$  most probable paths and prevent the exponential increase of the number of candidate paths.

To benefit from both approaches of error reduction, AED with constituent SCL decoders is an obvious solution [4]. However, the messages exchange is then limited to the constituent SCL decoder instances and, with one permutation per decoder core, the potential of automorphisms is not fully exploited. Furthermore, the selection of the most probable candidate in AED is already inherent in SCL decoding.

In [8], [9], near-ML performance was achieved for Reed-Muller codes by running SCL decoders on permutations of the channel LLRs and combining the different lists in each decoding step. Similarly, SCL decoding of Polar codes can benefit from the usage of automorphisms, which represent different noise realizations of the received channel data. For this purpose, an SCL- $L$  decoder is initialized with  $L$  permutations  $\pi_l, l \in [0, L)$  as

$$\boldsymbol{\alpha}^{0,l} = \pi_l(\text{LLR}(\mathbf{y})), \quad (5)$$

instead of only working on the original channel values corresponding to the identity permutation  $\pi_0(\text{LLR}(\mathbf{y}))$ . The permutations are sampled from the automorphism ECs of the code by a greedy selection method as described in [14]. Consequently, the list of candidates is filled from the start of SCL decoding and does not only start expanding with path splitting in the first nodes containing information bits.

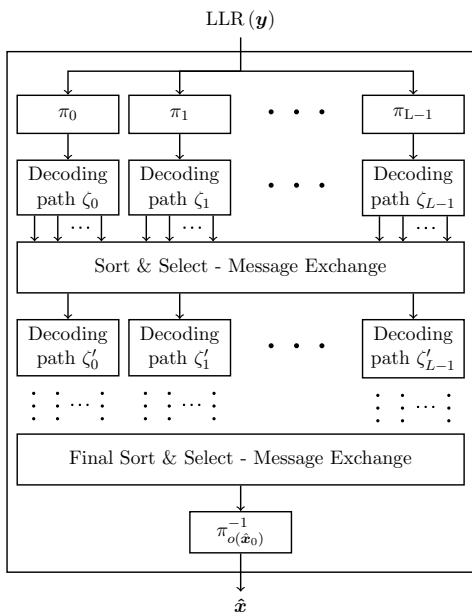


Fig. 1. SCAL decoding architecture

While the PMs of all candidates (i. e., decoding paths  $\zeta_l$ ) are already updated in the left-most frozen nodes, path splitting is superposed in non-frozen nodes. Thus, the different noise realizations of the permutations compete against each other whenever the expanded list of candidates is sorted and pruned to  $L$  in the sorters of the non-frozen nodes. This message exchange in the *Sort & Select* steps provides a gain compared to the independent decoding of the permutations in AED. Thus, SCAL has the ability to adapt to the channel conditions automatically, since either the candidates generated by path splitting or stemming from the permutations persist preferably.

Finally, the SCAL decoder outputs the most reliable candidate, i. e., the path with the smallest PM, which is found as the first entry (index 0) in the final sorted list of candidates. Depending on its origin  $o(\hat{x}_0)$ , the reverse permutation  $\pi_{o(\hat{x}_0)}^{-1}$  of the corresponding input permutation is applied as

$$\hat{x} = \pi_{o(\hat{x}_0)}^{-1} (\beta^{0,0}) \quad (6)$$

to obtain the decoded code word.

The architecture of an SCAL decoder is shown in Fig. 1 indicating the parallel decoding of paths  $\zeta_l$  until leaf nodes split the decoding paths. The decoding of each path  $\zeta$  produces multiple candidates. Based on the corresponding PMs, the *Sort & Select* step consolidates the  $L$  most reliable paths by the message exchange of the incoming candidate paths. It is noteworthy, that SCAL decoding can adopt the known, state-of-the-art optimizations for complexity reduction of SCL decoding without error-correction performance degradation.

#### IV. RESULTS

The results presented in this section are based on the polar code  $\mathcal{P}(128, 60)$  with  $\mathcal{I}_{\min} = \{27\}$ , which exhibits a block profile  $s = (3, 4)$  of its BLTA group and is therefore well suited for AED [14] and SCAL decoding. The permutation

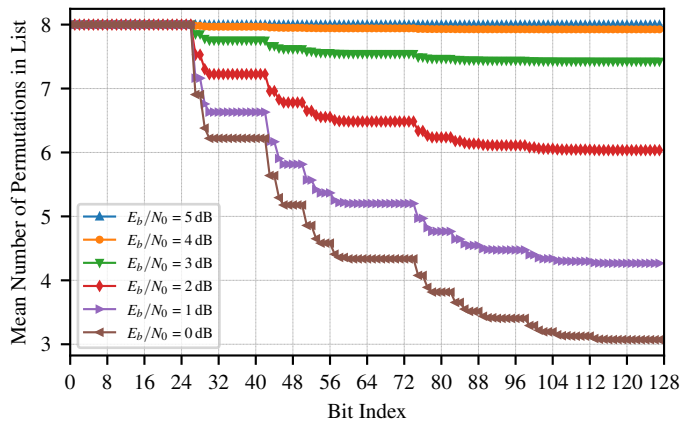


Fig. 2. Evolution of the number of different permutations  $\pi_l$  vs. the bit indices during SCAL-8 decoding of  $\mathcal{P}(128, 60)$

selection follows [14] to pick one automorphism from  $L$  ECs. Since the same code was used in [14], this selection enables a direct comparison to AED.

The Fast Simplified SCAL (Fast-SSCAL) and Fast Simplified Successive-Cancellation List (Fast-SSCL) decoders use optimized nodes according to [15], [16] and a quantization of 6 bit for LLRs and 8 bit for PMs, for both, Frame Error Rate (FER) simulations and hardware implementations.

Our simulation model applies Binary Phase Shift Keying (BPSK) modulation and uses an Additive White Gaussian Noise (AWGN) channel. Up to  $10^8$  pseudo-random blocks with a limit of  $10^3$  erroneous decoded block are simulated.

##### A. Analysis of Automorphism Evolution

To evaluate the novel SCAL decoding algorithm, the evolution of the permutations is analyzed. The permutations can be seen as different noise realizations, and the ones which are easier to decode prevail. Thus, the mean number of different permutations within the list of surviving candidates decreases during SCAL decoding. This effect is shown in Fig. 2 for the  $\mathcal{P}(128, 60)$  under SCAL-8 decoding at different Signal-to-Noise-Ratio (SNR) points. The figure also shows that the permutations dominate classical candidate generation in SCL decoding with increasing SNR.

Unlike in SCL decoding, the final code word candidates (after undoing the permutation) are not necessarily different in SCAL decoding. Fig. 3 shows the average number of unique code word candidates and the number of different permutations of the surviving paths before the final *Sort & Select* stage. For low SNR, a large list diversity can be observed, as the number of unique code word candidates is almost identical to the maximum number of paths  $L$ . However, these candidates stem from only a small number of permutations, indicating that the SCL branching dominates candidate generation in this regime. Conversely, at high SNR, the decoder only rarely branches and, thus, behaves more like AED where almost all  $L$  initial permutations survive until the final selection. However, this results in a low list diversity, as all decoding paths converge to the same (correct) code word candidate most of the time.

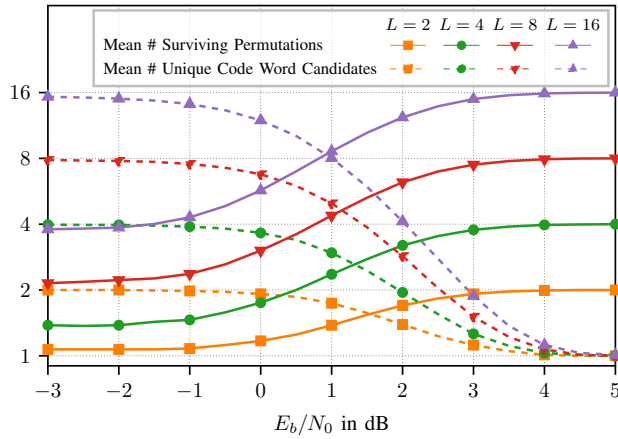


Fig. 3. Average number of unique final code word candidates and average number of permutations vs. SNR for SCAL decoding of  $\mathcal{P}(128, 60)$

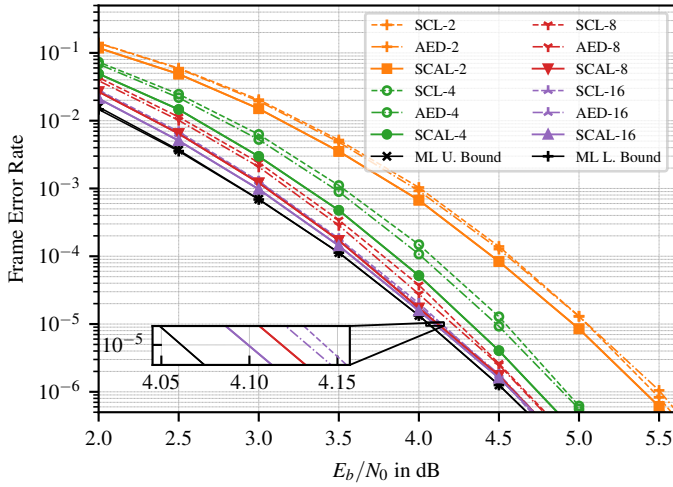


Fig. 4. FER vs. SNR for SCL, AED and SCAL decoding of  $\mathcal{P}(128, 60)$

### B. Error-Correction Performance

The plot in Fig. 4 shows the FERs of SCAL decoding, SCL decoding and AED for  $L/M \in \{2, 4, 8, 16\}$ . The upper and lower bounds for ML decoding performance are also given, which are observed by performing SCL decoding with  $L = 128$ . Whenever the decoded codeword is closer to the received channel values than the correct codeword, an ML decoder would fail. Thus, counting these cases provides the upper ML bound. Similarly, the lower bound is derived with the additional condition that the final list of candidates contains the correct codeword. In Fig. 4, both bounds coincide.

It can be seen that SCAL-2 provides a gain of 0.1 dB over AED and SCL decoding. At an FER of  $10^{-5}$ , SCAL-4 has a performance gain of 0.22 dB and 0.16 dB compared to SCL-4 and AED-4 and a gap of 0.074 dB and 0.11 dB to SCL-8 and AED-8, respectively. At the same FER, SCAL-8 outperforms SCL-16 and AED-16 by 0.024 dB and 0.015 dB, respectively, and the gap to the ML bound is 0.06 dB. To summarize, SCAL decoding outperforms the error-correction performance of AED and SCL decoding significantly for all list sizes/degrees of parallelism.

TABLE I  
IMPLEMENTATION RESULTS OF SCAL AND AE DECODERS

$M/L$	SCAL 4	AED 8	SCAL 8	AED 16
Frequency [MHz]	498	498	500	495
Throughput [Gbps]	63.8	63.7	64.0	63.3
Latency [ns]	48.2	22.1	64.0	22.2
Area [mm <sup>2</sup> ]	0.128	0.170	0.381	0.338
<b>Area Eff. [Gbps/mm<sup>2</sup>]</b>	<b>496.5</b>	<b>375.1</b>	<b>168.2</b>	<b>187.0</b>
Utilization [%]	72	74	72	73
Power Total [W]	0.194	0.320	0.552	0.640
<b>Energy Eff. [pJ/bit]</b>	<b>3.04</b>	<b>5.03</b>	<b>8.62</b>	<b>10.12</b>
Power Density [W/mm <sup>2</sup> ]	1.51	1.89	1.45	1.89

### C. Hardware Implementation

In addition to the improved error-correction performance, also the implementation costs of the proposed decoders have to be considered. Thus, we implemented different AED, SCL and SCAL decoders. All decoder implementations are unrolled and fully pipelined architectures for a target frequency of 500 MHz. Synthesis was executed with *Design Compiler* and Placement and Routing (PAR) with *IC-Compiler*, both from *Synopsys*, in a 12 nm FinFET technology from Global Foundries under worst case Process, Voltage and Temperature (PVT) conditions (125 °C, 0.72 V) for timing and nominal case PVT (25 °C, 0.8 V) for power. Power values stem from post-PAR netlist simulations with back-annotated wiring data and test data at  $E_b/N_0 = 4$  dB.

In fully pipelined architectures, the coded throughput is calculated as  $T_c = f \cdot N$ , with clock frequency  $f$ . Metrics for comparison are area efficiency  $\mu_A = T_c/A$ , energy efficiency  $\mu_E = P/T_c$ , with  $A$  being the area and  $P$  the power of the implementation, and power density  $P/A = \mu_E \cdot \mu_A$ .

#### 1) SCAL decoding vs. AED:

The PAR results for SCAL decoder and AED implementations are presented in Table I. For a fair comparison of the implementation costs of SCAL and AE decoders, the architectures having comparable error-correction performance are selected. Thus, SCAL-4 is compared with AED-8, and SCAL-8 with AED-16. It can be seen, that the SCAL decoders have a better energy efficiency than their AED counterparts. The area efficiency of SCAL-4 is  $1.32\times$  better than  $\mu_A$  of AED-8. Comparing  $\mu_A$  of SCAL-8 and AED-16, the SCAL decoder is  $0.90\times$  worse. All presented SCAL decoders have a better power density than AED. In terms of latency, AED is always at an advantage, since its latency is defined by the latency of the SC decoder cores.

#### 2) SCAL decoding vs. SCL decoding:

The comparison of SCAL and SCL decoder implementations aims for showing the overhead caused by generating and processing  $L$  permutations of the input LLRs in the SCAL decoder. Thus, two decoders with equal  $L$  are compared, respectively. The threshold parameters for the optimized Single Parity-Check (SPC) nodes [16] are set to preserve the error-correction performance of each decoder, i.e.,  $S_{\text{SPC}} = \{2, 2\}$  and  $k_{\text{SPC}} = \{2, 3\}$  for SCAL- $\{4, 8\}$ , and  $S_{\text{SPC}} = \{3, 4\}$  and

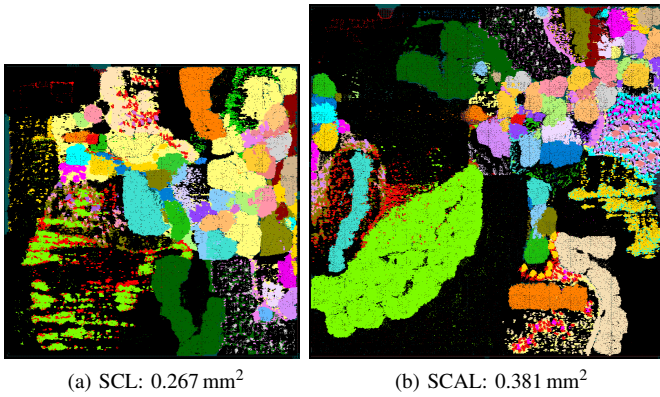


Fig. 5. Layouts of SCL-8 decoder [16] (a) and SCAL-8 decoder (b), both for  $\mathcal{P}(128, 60)$ ; different colors represent computational kernels, delay line memory is colored in black; the layouts have the same scaling.

TABLE II  
IMPLEMENTATION RESULTS OF SCAL AND SCL DECODERS

$L$	SCL 4	SCAL 4	SCL 8	SCAL 8
Frequency [MHz]	500	498	500	500
Throughput [Gbps]	64.0	63.8	64.0	64.0
Latency [ns]	44.0	48.2	62.0	64.0
Area [mm <sup>2</sup> ]	0.101	0.128	0.267	0.381
<b>Area Eff. [Gbps/mm<sup>2</sup>]</b>	<b>632.8</b>	<b>496.5</b>	<b>239.5</b>	<b>168.2</b>
Utilization [%]	73	72	73	72
Power Total [W]	0.161	0.194	0.434	0.552
<b>Energy Eff. [pJ/bit]</b>	<b>2.52</b>	<b>3.04</b>	<b>6.79</b>	<b>8.62</b>
Power Density [W/mm <sup>2</sup> ]	1.60	1.51	1.63	1.45

$k_{\text{SPC}} = \{2, 3\}$  for SCL- $\{4, 8\}$ , respectively. The corresponding results are given in Table II.

Fig. 5 shows the two layouts of the SCL-8 decoder (5a) and the SCAL-8 decoder (5b) with equal area scaling. Whenever possible, equal coloring is used for the computational kernels in both implementations. The most conspicuous difference is the size of the cells highlighted in lime-green, which correspond to the first  $g$ -function of the decoder in the root node. Since in the SCL decoder, only one input vector needs to be processed (in  $L$  variants), in SCAL decoding the input to this  $g$ -function is a list of  $L$  LLR vectors. The corresponding delay-line memory (colored in black for all stages) is also  $\times L$  greater. Thus, costs in area efficiencies are  $\mu_{\text{A, SCAL-4}} \approx \mu_{\text{A, SCL-4}} \times 0.78$  and  $\mu_{\text{A, SCAL-8}} \approx \mu_{\text{A, SCL-8}} \times 0.70$ , and in energy efficiencies  $\mu_{\text{E, SCAL-4}} \approx \mu_{\text{E, SCL-4}} \times 1.21$  and  $\mu_{\text{E, SCAL-8}} \approx \mu_{\text{E, SCL-8}} \times 1.27$ , respectively. However, the usage of the permutations brings a gain in the error-correction performance (section IV-B) for which reason SCAL decoders outperform comparable SCL decoders.

## V. CONCLUSION

In this paper, SCAL decoding is presented as a novel method to benefit from using automorphisms of polar codes together with SCL decoding. The proposed SCAL decoding algorithm outperforms AED and SCL decoding with respect to the error-correction performance. Regarding the hardware implementation costs, SCAL decoders benefit from the possible reduction

of the list size and therefore compete with AED and SCL decoder implementations with comparable error correction.

## REFERENCES

- [1] E. Arıkan, "Channel Polarization: A Method for Constructing Capacity-Achieving Codes for Symmetric Binary-Input Memoryless Channels," *IEEE Trans. Inf. Theory*, vol. 55, no. 7, pp. 3051–3073, Jul. 2009.
- [2] 3GPP, "NR; Multiplexing and channel coding," 3rd Generation Partnership Project (3GPP), Technical Specification (TS) 38.212, Apr. 2018.
- [3] I. Tal and A. Vardy, "List Decoding of Polar Codes," *IEEE*, vol. 61, no. 5, pp. 2213–2226, May 2015.
- [4] M. Geiselhart, A. Elkelesh, M. Ebada, S. Cammerer, and S. ten Brink, "Automorphism Ensemble Decoding of Reed–Muller Codes," *IEEE Trans. Commun.*, vol. 69, no. 10, pp. 6424–6438, Oct. 2021.
- [5] M. Geiselhart, A. Elkelesh, M. Ebada, S. Cammerer, and S. ten Brink, "On the Automorphism Group of Polar Codes," in *2021 IEEE Int. Symp. Inf. Theory ISIT*. Melbourne, Australia: IEEE, Jul. 2021, pp. 1230–1235.
- [6] Y. Li, H. Zhang, R. Li, J. Wang, W. Tong, G. Yan, and Z. Ma, "The Complete Affine Automorphism Group of Polar Codes," in *2021 IEEE Glob. Commun. Conf. GLOBECOM*. Madrid, Spain: IEEE, Dec. 2021, pp. 01–06.
- [7] C. Pillet, V. Bioglio, and I. Land, "Classification of Automorphisms for the Decoding of Polar Codes," in *ICC 2022 - IEEE Int. Conf. Commun.* Seoul, Korea, Republic of: IEEE, May 2022, pp. 110–115.
- [8] I. Dumer and K. Shabunov, "Soft-decision decoding of Reed-Muller codes: Recursive lists," *IEEE Trans. Inf. Theory*, vol. 52, no. 3, pp. 1260–1266, Mar. 2006.
- [9] N. Doan, S. A. Hashemi, and W. J. Gross, "Successive-Cancellation Decoding of Reed-Muller Codes With Fast Hadamard Transform," *IEEE Trans. Veh. Technol.*, vol. 71, no. 11, pp. 11 650–11 660, Nov. 2022.
- [10] M. Bardet, V. Dragoi, A. Otmani, and J.-P. Tillich, "Algebraic properties of polar codes from a new polynomial formalism," in *2016 IEEE Int. Symp. Inf. Theory ISIT*. Barcelona, Spain: IEEE, Jul. 2016, pp. 230–234.
- [11] A. Alamdar-Yazdi and F. R. Kschischang, "A Simplified Successive-Cancellation Decoder for Polar Codes," *IEEE*, vol. 15, no. 12, pp. 1378–1380, Dec. 2011.
- [12] C. Leroux, I. Tal, A. Vardy, and W. J. Gross, "Hardware architectures for successive cancellation decoding of polar codes," in *2011 IEEE Int. Conf. Acoust. Speech Signal Process. ICASSP*. Prague, Czech Republic: IEEE, May 2011, pp. 1665–1668.
- [13] A. Balatsoukas-Stimming, M. B. Parizi, and A. Burg, "LLR-based successive cancellation list decoding of polar codes," *IEEE Trans. Signal Process.*, vol. 63, no. 19, pp. 5165–5179, Oct. 2015.
- [14] C. Kestel, M. Geiselhart, L. Johannsen, S. ten Brink, and N. Wehn, "Automorphism Ensemble Polar Code Decoders for 6G URLLC," in *SCC 2023 13th Conf. Syst. Commun. Coding*. Braunschweig, Germany: IEEE, Feb. 2023.
- [15] L. Johannsen, C. Kestel, O. Griebel, T. Vogt, and N. Wehn, "Partial Order-Based Decoding of Rate-1 Nodes in Fast Simplified Successive-Cancellation List Decoders for Polar Codes," *Electronics*, vol. 11, no. 4, p. 560, Feb. 2022.
- [16] L. Johannsen, C. Kestel, T. Vogt, and N. Wehn, "Parallel Single Parity Check Nodes for High-Throughput Fast-SSCL Polar Code Decoders," in *2022 IEEE Symp. Future Telecommun. Technol. SOFTT*. Johor Bahru, Malaysia: IEEE, Nov. 2022, pp. 28–34.